A numerical study of a subtropical cloud free marine stable layer

By LAWRENCE N. LAHIFF, *Rosenstiel School of Marine and Atmospheric Science, Division of Atmospheric Science, University of Miami, Coral Gables, Florida 33124*

(Manuscript received May 4, 1973; revised version September 17, 1974)

ABSTRACT

The processes acting to stabilize or destabilize a parcel of air can be partitioned and their individual contribution to the time rate of change of stability can be examined as a forcing to a stability equation. This study examines the trade wind inversion and is different from previous studies on the subject in that time dependent solutions of three dimensional non-linear equations are explored here. A quasi-geostrophic model is developed to simulate a typical large-scale environment in which a stable layer develops. Large-scale divergence forcing is found to be comparable to horizontal advection of stabilities in regions to the east of a subtropical low-level anticyclone. The level of maximum divergence forcing is found to be elevated in regions of upward heat flux from the ocean. Longwave radiative cooling from water vapor will increase the stability if the amount of water vapor decreases rapidly through the stable layer, however, the radiation will decrease the stability if the water vapor is well mixed through the stable layer.

1. Introduction

During the summer months along the eastern and southern flanks of the subtropical high pressure areas in both the Atlantic and the Pacific Oceans a characteristic stable or inversion layer exists. The layer is so persistent that it exists in mean monthly climatological data for some stations. The purpose of this study is to examine some of the important physical processes that act in the formation and maintenance of this trade wind inversion.

The *Meteor* expedition collected a wealth of data on the low levels of the subtropical and tropical Atlantic atmosphere. The height of the base of the inversion was documented by Ficker (1936) from these data. These data show the lowest level of the inversion base to be at 15° N and 15° S near the west coast of Africa with the base rising to the west and toward the equator. Data from the *Meteor* showed the strength of the inversion to weaken and vertical moisture gradients to lessen toward the west and toward the equator (Riehl, 1954). Fig. 1 shows isopleths of the temperature increase from the base of the inversion to the top of the inversion. Since the thickness of the inversion changes very little in the horizontal the temperature increase is also a measure of the stability. The strength of the inversion is largest where the inversion is lowest with rapid weakening to the south and more gradual weakening to the west. Riehl (1954) notes that this weakening and lifting of the inversion takes place downstream along the streamlines. In the far western Atlantic the inversion is still found, but at a height of about 2 400 m near Puerto Rico (Langwell, 1948). Similar characteristics of the inversion have been found to exist in the eastern subtropical Pacific (Blake, 1928; Anderson, 1931; Blake, 1934; Neiburger et al., 1961; Haraguchi, 1968).

Riehl et al. (1951) have discussed the northeast trades of the Pacific Ocean. The data show the base of the inversion to increase in height from 900 mb at 135° W to 800 mb near Hawaii. Air enters the inversion from above conserving its potential temperature and air below the inversion has its potential temperature increase downstream along the streamlines, presumably from sensible heat transfer from the ocean. This lower air remains below the inversion on

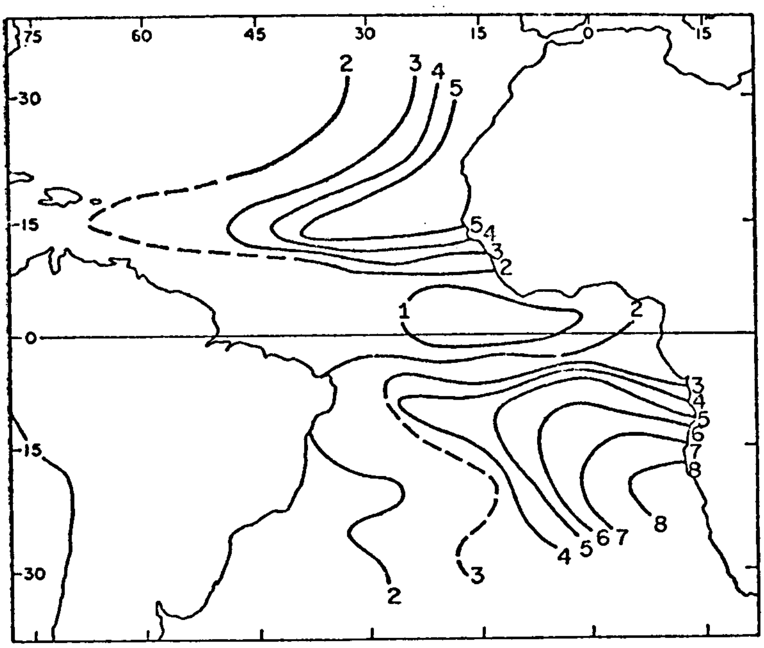

Fig. 1. Amount of temperature increase from bottom to top of inversion. Units °C. (Riehl, 1954.)

the large scale. The air below the inversion is moist, relative humidities of about 80 per cent, and the air above the inversion is dry, relative humidities of about 30 per cent.

The low level circulation in both the Atlantic and Pacific subtropics is dominated by the subtropical high pressure area. In both regions the high pressure is centered at 30° N latitude and about 30 degrees of longitude west of the coast. The coastal region underlies the eastern portion of the anticyclonic circulation. Riehl et al. (1951) have calculated the divergence and vertical velocity in the northeast trades and found a maximum of divergence at about 900 mb and sinking motion from 500 mb to the surface in the eastern part of the anticyclone. Neiburger et al. (1961) have found the maximum divergence is near the Californian and Mexican coasts with lesser values to the west and south.

Numerous explanations for the formation and maintenance of the inversion have been suggested. Petterssen (1938) states that the cool lower stratum is caused by radiation from either the top of a moist layer or the stratus cloud tops. Radiation cooling is advanced as the cooling mechanism rather than surface exchange cooling because of the unstable nature of the lower layer, lapse rates greater than moist adiabatic, which would be stable if cooled from below.

Ball (1960) presented a theory for the control of the inversion height by surface heating. Surface heating generates convective activity in the lowest layers and the convectively generated turbulent kinetic energy cannot be dissipated by viscous forces alone. A region of downward transfer of heat in the upper portion of the convective layer is suggested as being the method of destruction of this kinetic energy. Associated with this downward transfer of heat is a mass flux into the convective layer from the layer above, which is assumed non-turbulent and maintained in an inversion state by large scale subsidence. This mass flux would tend to thicken the convective layer and therefore raise the height of the inversion. This downward flux of heat is what Lilly (1968) refers to as the maximum entrainment hypothesis. The other hypothesis, no downward transfer of heat in the upper portion of the convective larger, is the minimum entrainment hypothesis. The latter assumption is used in this paper.

Lilly (1968) constructed a theoretical model of cloud topped mixed layers under a strong inversion. The model is horizontally homogeneous and subsidence in the upper layer and radiative flux at the top of the mixed layer are assumed known. Making use of thermal equations for the cloud layer and the cloud top, specifying the surface heat flux, and using the two different hypotheses for heat flux at the top of the cloud layer, he arrives at a closed set of equations for the inversion height and potential temperature in the cloud layer. After integrating these equations he obtains a nearly steady state solution which has an elevated inversion maintained by a balance of large scale sinking motion, turbulence in the cloud layer, and radiation from the cloud tops. Lilly also derives the equations for the case whan the phase change and latent heat released in the clouds are not neglected. The results show that the cloud layer is in active convection and the source of the energy is the latent heat evaporated from the sea surface and released in the cloud layers. Again an elevated inversion is found to result from a balance of radiation, convection, and large scale subsidence.

Lilly's work points out the important physical processes of the problem of maintenance and formation of the inversion, radiation, surface fluxes, and convection in the cloud layer. The model is simplified in that it is horizontally homogeneous and large scale environmental parameters must be specified. An extension of this work would be to include the the same physical processes but let the processes act in a time dependent large scale environment.

The purpose of this investigation is to develop a numerical model to study the effects that different physical processes, operating in a time dependent environment, have on the formation and maintenance of the trade wind inversion. A quasi-geostrophic model is developed for the large scale environment and radiation, surface fluxes of sensible and latent heat, and friction are parameterized as functions of the large scale dependent variables. A limitation of the model is that the subgrid scale fluxes of momentum, water vapor, and sensible heat vanish at a prescribed level in the model. Although this does not allow for the fluxes to interact with the trade wind inversion the model can investigate the response of the trade wind inversion to such surface fluxes. The atmosphere is also assumed to be cloud free, thus there is no effect of cloud mass flux. The effect of cloud detrainment and associated evaporative cooling at the base of the trade wind inversion may be very important in maintaining the sharpness of the inversion, but this effect is neglected in this cloud free study.

2. The stability equation

A stability equation will be derived in order to study what effect the different physical processes have on the time rate of change of stability.

The first law of thermodynamics as used in the numerical model is as follows:

$$\frac{\partial\theta}{\partial t} = -J(\psi,\theta) + \sigma\omega + \frac{1}{c_p}\left(\frac{p_0}{p}\right)^{R/c_p} Q \tag{1}$$

θ is the potential temperature, c_p is the specific heat of air at constant pressure, p_0 is a reference pressure (1 000 mb), R is the gas constant for dry air, p is the pressure, ψ is the streamfunction, Q is the diabatic heating, ω is the total time rate of change of pressure following a parcel, σ is the static stability, and J is the Jacobian operator. Operating on (1) with the vertical derivative with respect to pressure and assuming the thermal wind holds on the large scale we obtain the following:

$$\frac{\partial}{\partial t}\frac{\partial\theta}{\partial p} = -J\left(\psi,\frac{\partial\theta}{\partial p}\right) + \omega\frac{\partial\sigma}{\partial p} + \sigma\frac{\partial\omega}{\partial p} + \frac{1}{c_p}\left(\frac{p_0}{p}\right)^{R/c_p}\left[\frac{\partial Q}{\partial p} - \frac{RQ}{c_p p}\right] \tag{2}$$

The second term in the brackets in (2) can be ignored compared to the first term. We are dealing with the trade wind inversion located in the lower troposphere at a pressure of about 900 mb and the vertical scale on which the heating would act is on the order of 200 mb. Using these scales for the two terms in the brackets the first term is approximately 0.005 Q mb^{-1} and the second term is approximately 0.0003 Q mb^{-1}; therefore, the second term is dropped as being an order of magnitude smaller. We are now left with an equation for the time rate of change of stability of an air parcel as follows:

$$\frac{D\Gamma}{Dt} + \omega \frac{\partial \sigma}{\partial p} = -\sigma \frac{\partial \omega}{\partial p} - \frac{1}{c_p}\left[\frac{p_0}{p}\right]^{R/c_p} \frac{\partial Q}{\partial p} \tag{3}$$

Γ (a measure of the dry static stability) is the negative of the vertical derivative of potential temperature with respect to pressure and D/Dt is the derivative following a parcel excluding vertical motions.

From (3) it can be seen that a region of divergence would increase the stability of a parcel. This gives a basis for including the large-scale time dependent subtropical high pressure region with its associated downward motion and divergence to the east of it in the model. The second term on the right side of (3) shows that with the appropriate vertical distribution, diabatic heating can produce stability.

The processes operating to affect the stability can be examined through evaluation of the terms on the right side of (3). The diabatic effect on the stability can be examined by carrying out experiments which systematically include different diabatic effects.

3. The numerical model

A numerical model is developed to simulate a large-scale, three dimensional, time dependent environment in which a stable layer is formed and maintained. Some of the physical processes mentioned earlier are not able to be explicitly included in the model and must be arrived at implicitly by means of parameterization. This method determines the effect that small-scale motions have on the large scale structure by means of representing the small-scale effects as function of the large-scale dependent variables.

For the large-scale motions of interest a quasi-geostrophic model is used. The β-plane of the experiment is centered at 25° N and extends from 10° N to 40° N. In this region large-scale motions are well represented by the quasi-geostrophic approximation (Charney, 1963). Following Lorenz (1960) the complete vorticity, divergence, and thermodynamic equations may be reduced to form a quasi-geostrophic, simplified set of equations that, neglecting the diabatic and frictional effects, conserve the sum of kinetic plus available potential energy. The omega equation is formed by a combination of the vorticity and thermodynamic equation through a balance relation. The set of predictive equations and relations used are as follows:

$$\frac{\partial \nabla^2 \psi}{\partial t} = -J(\psi, \nabla^2 \psi + f) + f_0 \frac{\partial \omega}{\partial p} + F \tag{4}$$

$$\pi\sigma\nabla_\omega^2 + f_0^2 \frac{\partial^2 \omega}{\partial p^2} = f_0 \frac{\partial}{\partial p} J(\psi, \nabla^2 \psi) - f_0 \nabla^2 \left[J\left(\psi, \frac{\partial \psi}{\partial p}\right)\right] + f_0 \beta \frac{\partial}{\partial p}\frac{\partial \psi}{\partial x} + f_0 \frac{\partial F}{\partial p} - \frac{R}{c_p p} \nabla^2 Q \tag{5}$$

$$T = -\frac{f_0 p}{R} \frac{\partial \psi}{\partial p} \tag{6}$$

f is the coriolis parameter, f_0 is a constant coriolis parameter, F represents the effect of surface friction, π is $(R/p)(p/p_0)^{R/c_p}$, β is df/dy, ∇^2 is the Laplacian operatior, and T is temperature. The determination of Q and F will be discussed later in this section.

The static stability, σ, must be a function of pressure only. This is not inconsistent with the stability parameter Γ. Γ is allowed to vary freely both in space and time, it can be directly determined from the streamfunction through (6). Using data from Jordan (1958), a value for the change of potential temperature with pressure from a mean hurricane season sounding is about $-0.04°$ K mb^{-1} for 900 mb. Taking data from Riehl (1954), a value for this quantity is calculated to be $-0.08°$ K mb^{-1} in the inversion layer. The values for σ will be taken from Jordan's sounding and Γ can be expected to be as large as the data from Riehl indicates. The difference between the two is not so great as to introduce an error in the neglection of the time and horizontal space variation of σ in the thermal equation.

Because the evaluation of Q involves the moisture, the specific humidity is carried as a dependent variable. The moisture equation includes horizontal and vertical advection and evaporation from the sea surface. The equation used is as follows:

$$\frac{\partial q}{\partial t} = -J(\psi, q) - \omega \frac{\partial q}{\partial p} + E \tag{7}$$

q is the specific humidity and E is subgrid scale water vapor flux convergence due to evaporation.

The quasi-geostrophic set of equations must be applied at different levels in the vertical. The streamfunction is carried at 200 mb, 400 mb, 600 mb, 725 mb, 775 mb 825 mb, 875 mb, 925 mb, and 975 mb. The vertical velocity, temperature, and moisture are carried at 300 mb, 500 mb, 700 mb, 750 mb, 800 mb, 850 mb, 900 mb, and 950 mb. The moisture was also predicted at 1 000 mb. The vertical velocity is zero at 100 mb and 1 000 mb. The trade wind inversion is a phenomenon of the lower troposphere so the vertical resolution is high in the lower troposphere and is less resolved in the upper troposphere. From 1 000 mb to 700 mb a 50 mb resolution is used and from 700 mb to 100 mb a 200 mb resolution is used. Because the thickness of the trade wind inversion is nearly constant in space it is felt that a 50 mb resolution can adequately indicate the region where an inversion layer is present, although its marked intensity will not be resolved with such a vertical resolution. The horizontal grid is square with a mesh size of 2.5 degrees of latitude. The grid extends from 10° N to 40° N and from 10° W to 50° W. Strictly speaking, the east–west grid size should decrease with increasing latitude. The decrease of east–west distance is approximately 20 per cent from 10° N to 40° N. Because the initial data is picked from a mean August map over the oceans where the data itself is not highly accurate and the important features of the initial data are the large scale systems, which were retained, the picking of the initial data from a 2.5 degree latitude by 2.5 degree longitude grid to a square 2.5 degree mesh is not considered a serious error.

The east–west boundary conditions are cyclic. There is a region of eight grid points added to the initial data at the eastern end that is a linear interpolation of the data such that the last column of the cyclic region is equal to the first column of the data region. This is done only for the initial data. For time greater than $t = 0$, all values on the last column of the cyclic region are set equal to the values on the first column. This boundary condition essentially make the region of integration into a cylinder, so that flow which leaves one end of the grid enters from the other end. This boundary condition is used for all variables. Omega is set equal to zero at 1 000 mb and at 100 mb and is also set equal to zero along the north–south boundaries. The streamfunction needs only lateral boundary conditions. The north and south boundary values of streamfunction are constant in the east–west and in time. The effects of this condition are that of a non-viscous wall at the north and south boundaries of the model. The moisture is cyclic in the east–west and the north–south values are linearly extrapolated from the interior values.

All of the horizontal advection terms are evaluated by use of the Arakawa (1966) Jacobian. This technique is used because it conserves kinetic energy, mean square vorticity, and average wave number over the domain of integration. This is important in preventing computational instability caused by aliasing. The vorticity equation is a two-dimensional Poisson equation with horizontal boundary conditions. The method used to relax this equation is one that employs a Fourier analysis of the field and obtains the new value of streamfunction in one step. The omega equation must also be relaxed. This is a three-dimensional Poisson equation with lateral and top and bottom boundary conditions. The method used to relax the equation is successive overrelaxation. When a value of streamfunction is necessary at an intermediate level it is assumed to vary linearly with pressure. The time derivatives are computed by use of the Euler-backward scheme using a time step of one half hour (Matsuno, 1966).

Surface friction is parameterized in the vorticity equation and the effect is made proportional to a mean surface wind speed times the relative vorticity as follows:

$$F = \frac{C_D V}{DZ} \nabla^2 \psi$$

C_D is the drag coefficient (0.0001), V is a mean wind speed (10 ms^{-1}), and DZ is the mean thickness of the boundary layer (2 000 m). This relation for friction is obtained assuming a linearized form for the surface stress and assuming the effect linearly goes to zero at a height DZ. The coefficient of the vorticity is evaluated only once and has a value of $5 \times 10^{-7}\, s^{-1}$. Because of the high resolution in the lower levels of the model, friction is assumed to

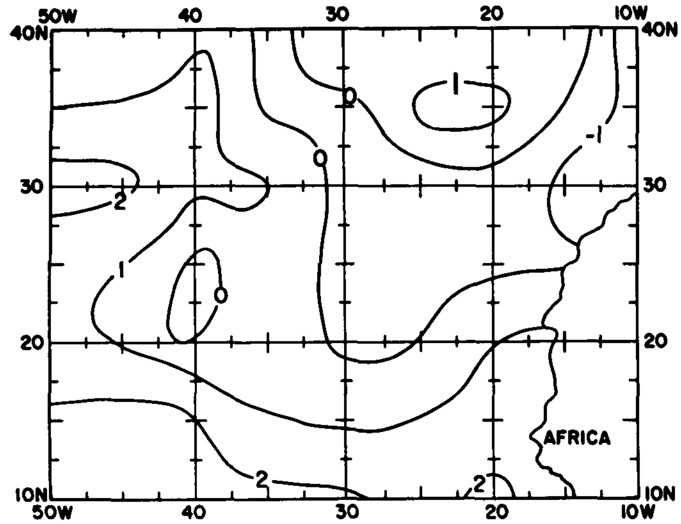

Fig. 2. Initial difference of water and air temperature. Positive values indicate warmer water. Units degrees centrigrade.

affect the lowest four levels, giving a frictional affected layer 175 mb thick.

Sensible heat transfer from the ocean surface is included. The formulation for Q_{sh} is given as follows:

$$Q_{sh} = g\frac{\partial F}{\partial p}$$

$$F = \begin{cases} F_s\dfrac{(P-800)}{200} & 800\,\text{mb} \leqslant p \leqslant 1\,000\,\text{mb} \\ 0 & p \end{cases}$$

$$F_s = C_s(T_w - T_a)\,V$$

T_w is the sea surface water temperature, T_a is the 1 000 mb air temperature, V is the wind speed at 975 mb, and C_s is a constant of proportionality for sensible heat transport (0.0329 mb K^{-1}). It is assumed that F is a linear function of pressure and vanishes at 800 mb. This assumes that turbulence will mix the sensible heat through the lowest three layers giving a 150 mb thick layer affected by sensible heat transport. This corresponds to the minimum entrainment hypothesis of Lilly (1968) and, therefore, there is no entrainment of heat from above the 800 mb level. The results of Lilly (1968) indicate that the results are similar for the two entrainment hypotheses. The sensible heat effect is assumed zero when the air temperature is warmer than the water temperature or in a region over land. The temperature difference between the ocean and the atmosphere is obtained by taking the difference between August water temperatures obtained from the Morskai Atlas (1953) and August air temperatures (Crutcher & Meserve, 1970). The model does not predict temperature at the surface, so a vertical linear extrapolation is made to the surface from the interior two points. The sea surface temperature is calculated from these model surface temperatures by adding the observed air-water temperature difference. This is done for the initial time only. This derived sea surface temperature field is assumed constant in time and the flux of heat is proportional to the difference of the time dependent extrapolated surface air temperatures and the derived sea surface temperatures. The initial air-water temperature difference field is shown in Fig. 2.

Evaporation from the ocean surface is taken into account. The effect is made proportional to the wind speed times the difference of the saturated specific humidity at the sea surface temperature and the specific humidity of the air at 1 000 mb as follows:

$$E = g\frac{\partial F}{\partial p}$$

$$F = \begin{cases} F_e \dfrac{(P - 800\ \text{mb})}{200} & 800\ \text{mb} \leqslant p \leqslant 1\ 000\ \text{mb} \\ 0 & p < 800\ \text{mb} \end{cases}$$

$$F_e = C_e(q_s - q_a)\ V$$

q_s is the saturated specific humidity at the sea surface temperature, q_a is the specific humidity of the air at 1 000 mb, and C_e is a constant of proportionality for evaporation (1.71×10^{-5} mb $s^2\ m^{-1}$). It is assumed that F is a linear function of pressure which vanishes at 800 mb. This gives a layer affected by evaporation 150 mb thick. Evaporation is assumed equal to zero if the specific humidity is greater than the saturated sea surface temperature specific humidity or if the region is over land. It has been assessed that these bulk aerodynamic formulae for evaporation and heating are applicable for transfers over the oceans and beneath an inversion (Priestley & Taylor, 1972).

Radiation is included in the model following Danard (1969). The method includes only longwave radiation from water vapor. Shortwave radiation is not included because the magnitude of its effect is considered to be less than one half of that of longwave radiation (Davis, 1963). Although shortwave radiation is small the model must be considered a nighttime model of the physical processes affecting the inversion layer. Danard (1969) demonstrates that shortwave radiation is a smaller effect than longwave radiation. Longwave cooling from carbon dioxide is found to be small compared to cooling due to water vapor. Cooling of 0.2°C day^{-1} due to carbon dioxide compared to cooling of 1.2°C day^{-1} due to water vapor was found for a cloudless troposphere (Manabe & Moller, 1961). Because of the above, only longwave cooling from water vapor is considered. The radiative fluxes are evaluated at the levels of the streamfunction so that Q is calculated at the omega levels. In this case Q_r is evaluated from the following:

$$Q_r = -g\frac{\partial F^*}{\partial p}$$

F^* is the longwave radiative flux due to water vapor.

The effect of radiation on different temperature and moisture profiles is shown by Staley & Jurica (1968). It is demonstrated that in a moist inversion, one in which the dew point decreases regularly through the temperature inversion, radiation has the effect of destroying the stability. In a dry inversion, one in which the dew point drops nearly 40°C in 50 mb through the inversion, the stability is increased due to radiation. In the first case the warm layer has a larger flux divergence than any other layer so that the inversion is decreased in intensity. In the second case there is a net upward radiation from the moist layer so that the lower portion of the inversion is cooled. Both cases show no tendency to either raise or lower the inversion, radiation only acts to increase or decrease its intensity.

Initial data used for the model are mean August data taken from Crutcher & Meserve (1970). The surface pressure and heights of the 850 mb, 700 mb, 500 mb, 300 mb, 200 mb, and 100 mb surfaces were picked over the limited region of 10° W to 50° W and 10° N to 40° N. The temperature and dew point temperature were also extracted at the surface, 850 mb, 700 mb, and 500 mb over the same limited region. From the temperature and dew point data values of the specific humidity were calculated at the surface, 850 mb, 700 mb, and 500 mb.

The heights of the levels used for streamfunction in the model were evaluated by interpolation of the data. The initial data correspond closely to the observed flow pattern, the observed temperature structure, and the observed moisture pattern in this region when a trade wind inversion layer is evident.

4. Motion and moisture field results

The experiments were conducted so as to separate the physical processes involved in the formation and maintenance of the inversion. This was accomplished by starting with a basic experiment followed by further experiments with different physical processes added to the model. The integration period in model time was 120 hours. Experiment I consisted of the integration of the quasi-geostrophic equations with no parameterized effects. Experiment II was carried out with the addition of sensible

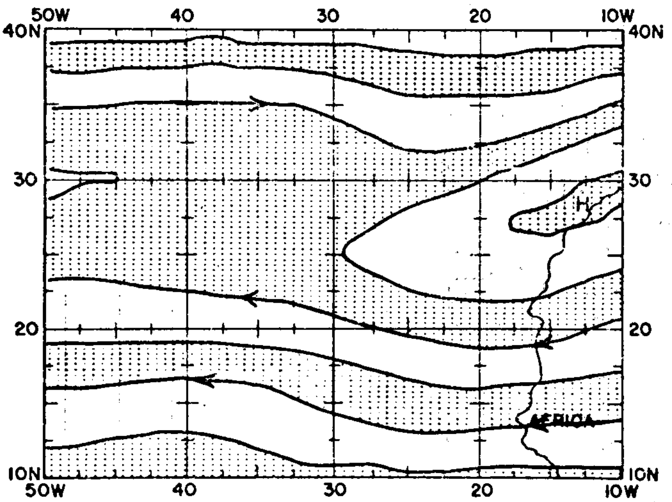

Fig. 3. Streamfunction at 600 mb. Experiment I after 120 hours of integration. Isopleth interval is 25×10^5 m^2 s^{-1}. The letter *H* indicates a center of anticyclonic circulation. The letter *L* indicates a center of cyclonic circulation.

heat transport from the ocean surface. Radiation and heat transport were the parameterized effects in Experiment III. Other experiments were conducted and a detailed discussion of each is presented in Lahiff (1971).

The initial data represents a hypothetical initial state taken from climatology. The model is intended to demonstrate the effect of different physical processes acting in the time dependent environment generated from these initial data. The model cannot be expected to reproduce climatology because the subtropical anticyclone is a longwave feature of the global circulation and the processes that maintain it are not found in the limited area of the high pressure itself. A real case study is not made because of a lack of complete observations on a synoptic scale in this region. Fig. 3 and Fig. 4 depict the

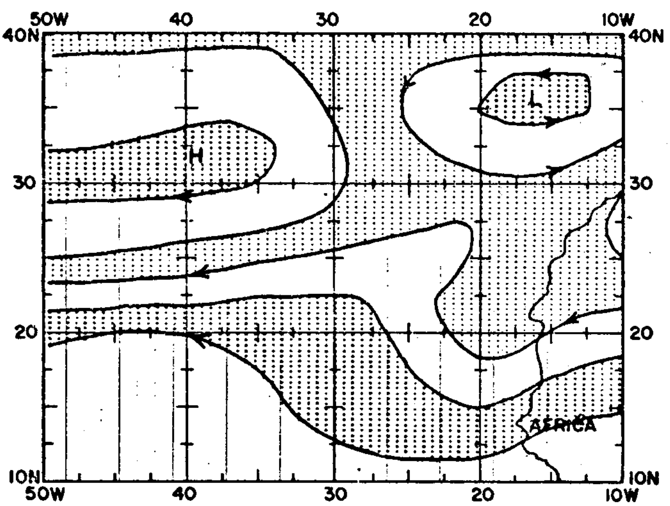

Fig. 4. Streamfunction at 975 mb. Experiment I after 120 hours of integration. Isopleth interval is 25×10^5 m^2 s^{-1}. The letter *H* indicates a center of anticyclonic circulation. The letter *L* indicates a center of cyclonic circulation.

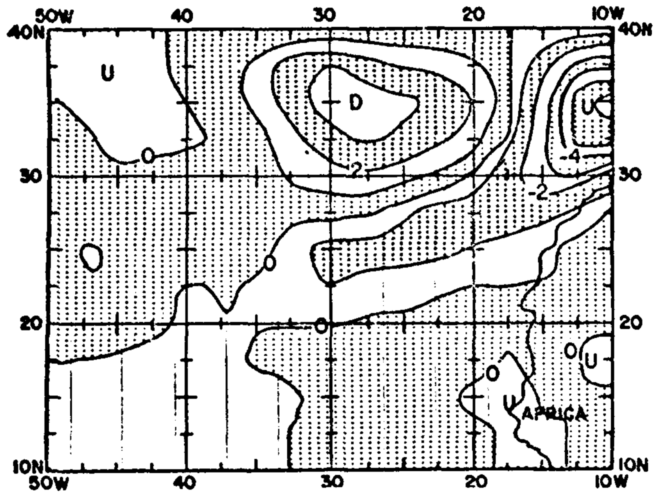

Fig. 5. Vertical velocity at 700 mb. Experiment II after 96 hours of integration. Isopleth interval is 1.0×10^{-4} mb s^{-1}. The letter *U* indicates a center of upward motion and the letter *D* indicates a center of downward motion.

streamfunction field after 120 hours of integration in Experiment I. At the 975 mb level the subtropical anticyclone is evident and at 600 mb the general ridging through the center of the region is present. The resulting flow pattern is not unrealistic for the area.

Fig. 5 represents the vertical motion field at 700 mb after four days of integration in Experiment II. There is large scale sinking motion to the east of the subtropical anticyclone. The rising motion near the eastern boundary is produced by the cyclonic flow pattern located in the northeast. The general subsidence and the horizontal motion to the east of the anticyclone causes a large dry region to form in the northeast (Fig. 6). The descending and dry air is found to be essential in forming and maintaining the inversion. The results of the experiments in terms of the motion fields are all somewhat similar and the differences are

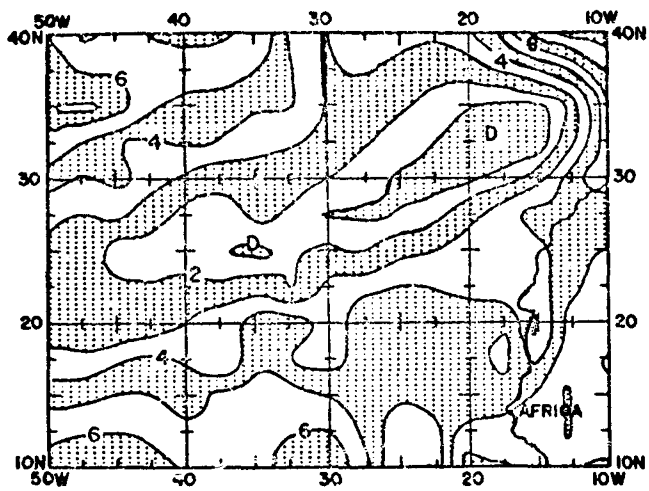

Fig. 6. Specific humidity at 800 mb. Experiment III after 96 hours of integration. Isopleth interval is 1.0 gram $kilogram^{-1}$. The letter *D* indicates a relative minimum of moisture and the letter *M* indicates a relative maximum of moisture.

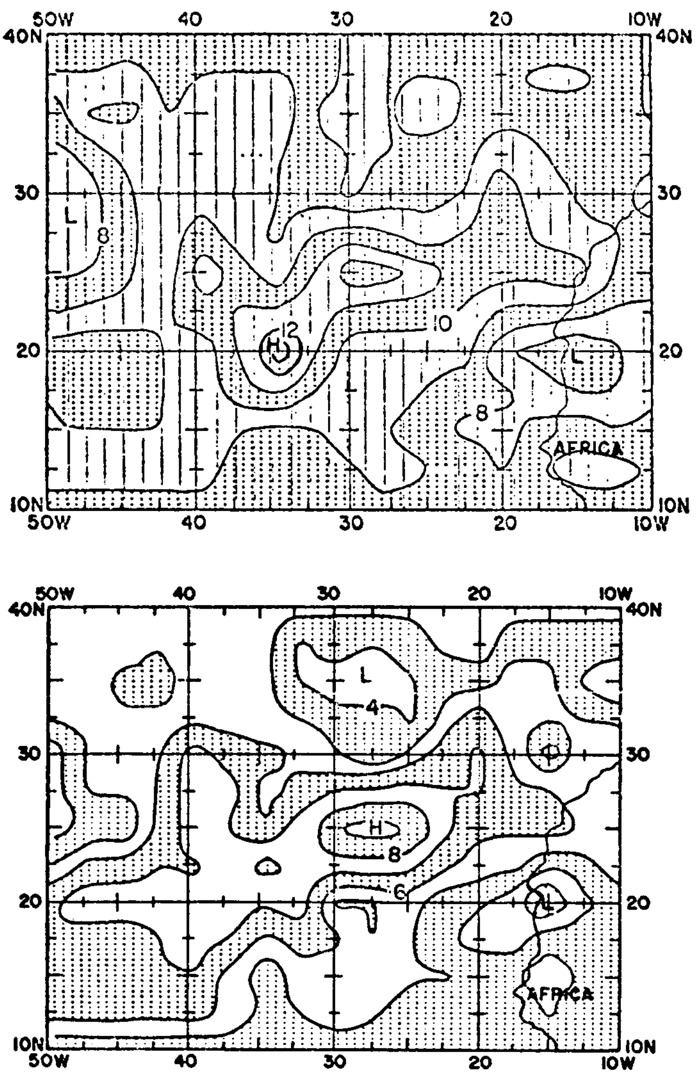

Fig. 7. Initial stabilities. Top at 850 mb and bottom at 900 mb. Isopleth interval is 1.0×10^{-2} °K mb^{-1}. The letter *H* indicates high values of stability and the letter *L* indicates low values of stability.

more evident in the derived quantities such as temperature and stability.

Moisture and heat balances were calculated and compared to Riehl et al. (1959) and Riehl & Malkus (1956) in order to provide a check on the model and the parameterizations. Balances are calculated over a trajectory in the lower trades. Details of the calculations are presented in Lahiff (1971). The model is in agreement with observations with the trades exporting both sensible and latent heat with latent heat export being larger.

5. Stability field results

The effect that each of the physical processes has on the stability of an air parcel can be found by examining the differences among the experiments and by evaluating the terms on the right side of the stability equation (3).

The initial stability fields at 850 mb and 900 mb both indicate maximum stability in the central portion of the integration area (Fig. 7). This region of maximum stability is oriented along the streamlines.

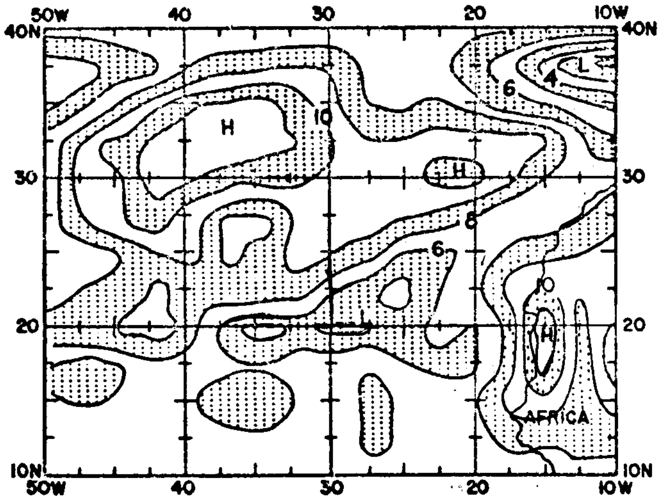

Fig. 8. Stability at 850 mb for Experiment II after 120 hours of integration. Isopleth interval is 1.0×10^{-2} °K mb^{-1}. The letter *H* indicates high values of stability and the letter *L* indicates low values of stability.

Experiment I includes no parameterized effects, therefore, divergence and advection are the dynamic processes acting to change the stability at a point. After integrating the model for five days it is noted that the stabilities at 850 mb decreased in intensity and were advected to the southwest, whereas the stabilities at 900 mb decreased only slightly and remained nearly stationary. It is found by evaluating (3) at different levels that the maximum contribution to the production of stability due to divergence is to the east of the subtropical anticyclone and in the lowest level. Outside of this region the divergence contributes little to the formation of stabilities. The lowest level can maintain, against advection, a region of above average stability due to the divergence associated with the subtropical high pressure area and in other regions the initial stabilities weaken and are advected downstream.

Transport of sensible heat from the ocean surface is included in Experiment II. The result of sensible heat transport is to cause rising motion or lessen the sinking motion near the surface. This leads to a raised and in some regions an enhanced level of maximum divergence. Evaluation of the divergence effect in (3) for Experiment II reveals that the levels just above the lowest level are the levels where production of stability is favored. Fig. 8 is the stability field at 850 mb after five days of integration and it can be seen that the stability to the east of the subtropical anticyclone decreases only slightly from the initial values (Fig. 7).

The sensible heat transport near the African coast is large and produces an elevated inversion layer. The air water temperature difference in this region approaches 2° K, hence a large flux of heat is realized. Fig. 9 shows a time series of soundings off the African coast and the development of this stable layer can be seen. The heating near the surface produces upward motion which decays with height producing a level of strong divergence near 825 mb. The sensible heat transport has the smallest effect in the northeast where the sea surface temperatures are rather cool and has its largest effect over the open ocean where the sea temperatures are warm. Where the sensible heat transport is large it produces slight convergence near the surface and weakens the stability near the surface. This combination of location and effect causes the sensible heat transport to raise the level of stability downstream.

The inclusion of longwave cooling from water vapor in Experiment III greatly enhances the production of stability in the northeast portion of the integration area. The subsidence to the east of the subtropical anticyclone leads to very dry air in the mid and upper levels. Radiation will then produce strong cooling from the top

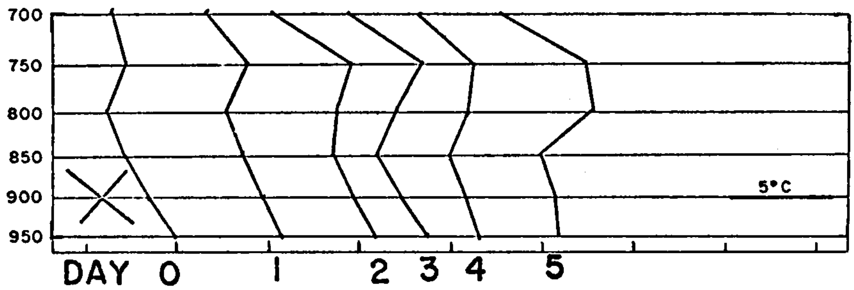

Fig. 9. Time series from Experiment II of soundings off the African coast where sensible heat transport is large. Plotted on a skew-T log P diagram.

of the lowest moist layer in these regions. The stabilities at 850 mb and 900 mb after five days of integration are shown in Fig. 10. Comparison of Fig. 10 with observations (Fig. 1) demonstrates that the patterns are similar, the region of maximum stability in the model is found north of the observed stability. The model is based on hypothetical, smoothed data and there exist very few observations, therefore the comparison should be made between the patterns of stability. Comparison of Fig. 8 and Fig. 10 reveal a marked difference in stabilities in the center of the subtropical anticyclone and an enhancement of the stabilities in the trade wind region. Upon examination of the radiation contribution to the change in stabilities in (3) it is found that radiation weakens the stability in the subtropical anticyclone. In the anticyclone the moisture is well mixed in the vertical and, in agreement with Staley & Jurica (1968), the stabilities are decreased due to radiation.

6. Summary and conclusions

In spite of the limitations of the model used, that is the quasi-geostrophic assumption, the need to parameterize the small scale motions, and a cloud free situation, the results are in agreement with observations. The experiment with no parameterized effects revealed that divergence and horizontal advection are of the same importance in producing stability in the eastern portion of the subtropical high pressure. Outside of this region the vertical velocities are very small and the divergence is no longer important in producing stability. In the eastern portion of the subtropical anticyclone the divergence produces stability in the lowest layer and maintains initial stabilities against the advection in this region. This agrees with observations which show the stability to be largest in the eastern portion of the anticyclone.

The experiment that included the effect of sensible heat transport showed significant results. The sensible heat transport is capable of producing an elevated and more intense stable layer. The sensible heat transport forces either an upward motion or a decrease in the sinking motion near the surface which elevates the level of maximum divergence. This causes the greatest production of stability at an elevated level and also increases the magnitude of the divergence to make it a significant factor in the trades. In the eastern portion of the subtropical anticyclone the ocean surface is rather cool and sensible heat transport will not elevate the level of maximum stability production. The sensible heat transport leads to the classic lifting of the inversion downstream. It must be kept in mind that the vertical extent of the subgrid scale fluxes vanishes at a fixed height and hence does not allow for interction with the trade wind inversion, but the model can demonstrate the relative effectiveness of these type of subgrid scale fluxes on the stable layer.

Radiation when coupled with a rapid decrease of moisture in the vertical will increase the intensity of the inversion and has an effect comparable to both horizontal advection and divergence. The existence of the rapid decrease of moisture is important or radiation will weaken the stable layer. The sharp gradient of moisture is most likely to occcur near the surface in a region of sinking motion where divergence is acting to produce stability. In these regions the combination of radiation and divergence can

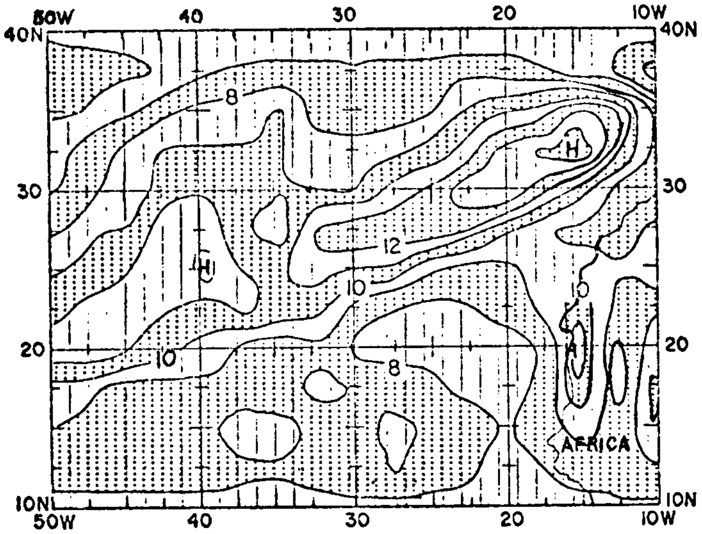

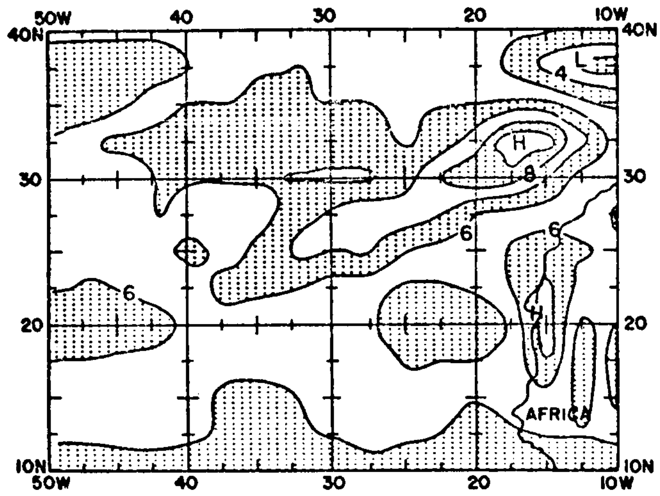

Fig. 10. Stability after 120 hours of integration for Experiment III. Top is 850 mb and bottom is 900 mb. Isopleth interval is 1.0×10^{-2} °K mb^{-1}. The letter *H* indicates high values of stability and the letter *L* indicates low values of stability.

produce the strong inversion that has been noted in observations. In the trades and the subtropical anticyclone the moisture is more thoroughly mixed in the vertical and the radiation effects weakens stability in these regions.

Observations that would be required to forecast the trade wind inversion would be winds and moisture. These values could be used as input to a quasi-geostrophic model that would include sensible heat transport and radiation. The forecast time could be increased if some parameterized effect could be found to halt the retrogression of the large scale features as was used in Krishnamurti et al. (1970).

Acknowledgements

It is a pleasure to thank Professor T. N. Krishnamurti for the many helpful suggestions and discussions concerning this research. Professor N. E. LaSeur is acknowledged for his helpful suggestions concerning the vertical structure of the model. The author is indebted to Rosa Sotolongo for typing the manuscript.

Partial financial support was provided by the National Science Foundation under Grants NSF GA-17822, NSF DES 7201509-02, and the Department of Defense Contract No. DAAB07-69-C-0062. The research was carried out while the author was a National Defense Education Act Fellow.

All computatins were carried out at the Florida State University Computing Center.

REFERENCES

Anderson, J. B. 1931. Observations from airplanes of cloud and fog conditions along the southern California coast. *Mon. Wea. Rev. 59*, 264–270.

Arakawa, A. 1966. Computational design for long term numerical integration of the equations of motion: Two-dimensional incompressible flow, Part I. *J Comp. Phys. 1*, 119–143.

Ball, F. K. 1960. Control of inversion height by surface heating. *Quart. J. Roy. Meteor. Soc. 86*, 483–494.

Blake, D. 1928. Temperature inversions at San Diego, as deduced from aerographical observations by airplanes. *Mon. Wea. Rev. 56*, 221–244.

Blake, D. 1934. Further conclusions from additional observations in the free air over San Diego, California. *Mon. Wea. Rev. 62*, 195–199.

Charney, J. 1963. A note on large scale motions in the tropics. *J. Atmos. Sci. 20*, 607–609.

Crutcher, H. S. & Meserve, J. M. 1970. *Selected level height, temperatures and dew points for the northern hemisphere.* NAVAIR 50-1C-52.

Danard, M. B. 1969. A simple method of including longwave radiation in a tropospheric numerical prediction model. *Mon. Wea. Rev. 97*, 77–85.

Davis, P. A. 1963. An analysis of the atmospheric heat budget. *J. Atmos. Sci. 20*, 5–22.

Ficker, J. 1936. Illustration. Veroff. Meteor, Inst., Berling, vol. 1, no. 4, 1936. (Reproduced in Riehl, H., 1954: *Tropical meteorology*, McGraw-Hill, New York, 392 pp.)

Haraguchi, P. Y. 1968. Inversions over the tropical eastern Pacific Ocean. *Mon. Wea. Rev. 96*, 177–185.

Jordan, C. L. 1958. Mean soundings for the West Indies area. *J. Meteor. 15*, 91–97.

Krishnamurti, T. N., Jarvinen, B., Kemper, J. E. & Abbott, D. A. 1970. Eddy motions in a tropical general circulation experiment with zonally asymmetric heating. *Proceedings of the Symposium on Tropical Meteorology*, Univ. of Hawaii, Honolulu, pp. MIV-1–1M1V-3.

Lorenz, E. N. 1960. Energy and numerical weather prediction. *Tellus 12*, 364–373.

Lahiff, L. N. 1971. A numerical study of a subtropical marine stable layer. Ph. D. dissertation, Florida State University, Tallahassee.

Langwell, P. A. 1948. Inhomogeneities of turbulence, temperature, and moisture in the West Indies trade wind region. *J. Meteor. 5*, 243–246.

Lilly, D. K. 1968. Models of cloud topped mixed layers under strong inversion. *Quart. J. Roy. Meteor. Soc. 94*, 292–309.

Manabe, S. & Moller, F. 1961. On the radiative equilibrium and heat balance in the atmosphere. *Mon. Wea. Rev. 89*, 503–532.

Matsuno, T. 1966. A finite difference scheme for time integrations of oscillatory equations with second order accuracy and sharp cut-off for high frequencies. *J. Meteor. Soc. Japan 44*, 85–88.

Morskoi Atlas, 1953. Russian Marine Atlas, II, Plate 17.

Neiburger, M., Johnson, D. S. & Chien, D. 1961. Studies of the structure of the atmosphere over the eastern Pacific Ocean in summer. I. The inversion over eastern North Pacific Ocean. *Univ. of Calif. Publications in Meteorology 1*, No. 1.

Petterssen, S. 1938. On the causes and the forecasting of the California fog. *Bull. Amer. Meteor. Soc. 19*, 49–55.

Priestley, C. H. B. & Taylor, R. J. 1972. On the assessment of surface heat flux and evaporation using large-scale parameters. *Mon. Wea. Rev. 100*, 81–92.

Riehl, H. 1954. *Tropical meteorology*. McGraw-Hill, New York, 392 pp.

Riehl, H. & Malkus, J. S. 1958. On the heat balance and maintenance of circulation in the trades. *Quart. J. Roy. Meteor. Soc. 82*, 21–29.

Riehl, H., Yeh, T. C., Malkus, J. S. & LaSeur, N. E. 1951. The northeast trade of the Pacific Ocean. *Quart. J. Roy. Meteor. Soc. 77*, 598–626.

Staley, D. O. & Jurica, G. M. 1968. Radiative modification of selected vertical temperature distribution. *Quart. J. Roy. Meteor. Soc. 94*, 310–317.

ЧИСЛЕННОЕ ИЗУЧЕНИЕ УСТОЙЧИВОГО ПРИВОДНОГО СЛОЯ В СУБТРОПИЧЕСКИЙ ОБЛАСТИ, СВОБОДНОЙ ОТ ОБЛАКОВ

Процессы, стабилизирующие и дестабилизирующие частицу воздуха, могут быть разделены и их индивидуальный вклад в скорость изменения устойчивости можно изучать, рассматривая эти процессы как возбуждение в уравнении для устойчивости. Здесь изучается пассатная инверсия и в отличие от предыдущих исследований используются нестационарные решения трехмерного нелинейного уравнения. *Для* моделирования типичного крупномасштабного окружения, в котором развивается устойчивый слой, стро-

ится квазигеострофическая модель. Найдено, что возбуждение за счет крупномасштабной дивергенции сравнимо с горизонтальной адвекцией устойчивости в областях к востоку от субтропического антициклона на нижних уровнях. Найдено, что уровень максимального возбуждения за счет дивергенции поднят в районах направленного вверх потока тепла от океана. Длинноволновое радиационное выхолаживание водяного пара быстро падает с высотой в устойчивом слое, однако, радиация будет уменьшать устойчивость, если водяной пар в устойчивом слое хорошо перемешан.